BIOCHEMISTRY
including biophysical chemistry & molecular biology

Article

pubs.acs.org/biochemistry

The Nuclear Magnetic Resonance Solution Structure of the Synthetic AhPDF1.1b Plant Defensin Evidences the Structural Feature within the γ-Motif

Fanny Meindre,[†] Dominique Lelièvre,[†] Karine Loth,[†] Oriane Mith,[‡] Vincent Aucagne,[†] Pierre Berthomieu,[‡] Laurence Marquès,[‡] Agnès F. Delmas,[†] Céline Landon,[†] and Françoise Paquet*[,†]

[†]Centre de Biophysique Moléculaire, CNRS UPR4301, Rue Charles Sadron, 45071 Orléans Cedex 2, France

[‡]Laboratoire de Biochimie & Physiologie Moléculaire des Plantes, INRA/SupAgro, 2 Place P. Viala, 34060 Montpellier Cedex 2, France

Supporting Information

ABSTRACT: Plant defensins (PDF) are cysteine-rich peptides that are major actors in the innate immunity in plants. Besides their antifungal activity, some PDF such as *Arabidopsis halleri* PDF1.1b confer zinc tolerance in plants. Here we present (i) an efficient protocol for the production of AhPDF1.1b by solid-phase peptide synthesis followed by controlled oxidative folding to obtain the highly pure native form of the defensin and (ii) the three-dimensional (3D) nuclear magnetic resonance structure of AhPDF1.1b, the first 3D structure of plant defensin obtained with a synthetic peptide. Its fold is organized around the typical cysteine-stabilized α-helix β-sheet motif and contains the γ-core motif involved in the antifungal activity of all plant defensins. On the basis of our structural analysis of AhPDF1 defensins combined with previous biological data for antifungal and zinc tolerance activities, we established the essential role of *cis*-Pro41 within the γ-core. In fact, the four consecutive residues (Val39-Phe40-Pro41-Ala42) are strictly conserved for plant defensins able to tolerate zinc. We hypothesized that structural and/or dynamic features of this sequence are related to the ability of the defensin to chelate zinc.

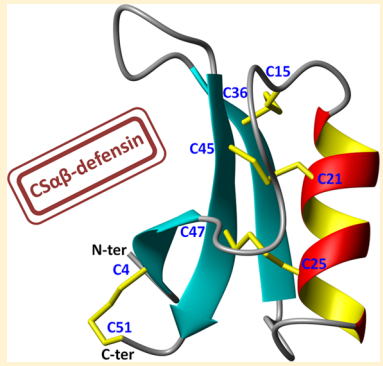

Defensins form a widespread and heterogeneous family of antimicrobial peptides (AMP) that are actively involved in the innate immunity in all organisms, including insects, plants, and mammals.[1] We focused here on plant defensins, whose antifungal activity is the most frequently reported in the literature.[2,3] Identified in most plant tissues, the peptide sequences (45−54 amino acids) harbor eight highly conserved cysteines involved in four conserved disulfide bonds (C1−C8, C2−C5, C3−C6, and C4−C7). Despite weak sequence identity, all plant defensins share a common globular cysteine-stabilized α-helix β-sheet structure (CSαβ)[4] also found in scorpion toxins and insect defensins,[5] which distinguishes them from vertebrate defensins (subdivided into three families, α-, β-, and θ-defensins).[6,7] Currently, 13 three-dimensional (3D) structures of plant defensins, either extracted or recombinant, are available in the Protein Data Bank (PDB). (i) The γ 1-hordothionin (PDB entry 1GPS),[8] the γ 1-purothionin (PDB entry 1GPT),[8] the RsAFP1 defensin (PDB entry 1AYJ),[9] the AhAMP1 defensin (PDB entry 1BK8),[10] the Psd1 defensin (PDB entry 1JKZ),[11] and the VrD1/VrD2 defensins (PDB entries 1TI5 and 2GL1)[12,13] were extracted from seeds of *Hordeum vulgare*, *Triticum aestivum*, *Raphanus sativus*, *Aesculus hippocastanum*, *Pisum sativum*, and *Vigna radiata*, respectively. (ii) The NaD1 defensin (PDB entries 1MR4, 4AAZ, and 4ABO)[14,15] and the PhD1 defensin (PDB entry 1N4N)[16] were purified from *Nicotiana alata* and *Petunia hybrid* flowers, respectively. (iii) The *Pachyrrhizus erosus* defensin SPE10 (PDB entry 3PSM)[17] and the *Medicago truncatula* defensin MtDef4 (PDB entry 2LR3)[18] were expressed in *Pichia pastoris*. (iv) The *Saccharum officinarum* defensin Sd5 (PDB entry 2KSK)[19] and the *Lens culinaris* defensin Lcdef (PDB entry 2LJ7) were expressed in *Escherichia coli*. The eight cysteine residues involved in four conserved disulfide bridges and a glycine in the γ-core motif are strictly conserved. The γ-core motif GXC(X_{3-9})C (X being any amino acid) consists of two antiparallel β-strands (β2 and β3) with an interposed β2−β3 loop. It includes two cysteine residues from two different bridges and is considered as a major determinant for the antifungal activity.[20]

Besides their antifungal activity, some plant defensins also exhibit unrelated activities, such as enzyme inhibition, translation inhibition, ion channel inhibition, or redox activity.[21−23] In addition, some plant defensins from subfamily 1 (PDF1) have been shown to confer zinc tolerance in yeast and in plant cells upon being overexpressed.[24] The AhPDF1.1b defensin had thereby been identified from a functional screening of an *Arabidopsis halleri* cDNA library in *Saccharomyces cerevisiae* yeast.[24] The *A. halleri* AhPDF1.1b was first produced in *E. coli*

Received: October 13, 2014
Revised: November 24, 2014
Published: November 24, 2014

dx.doi.org/10.1021/bi501285k | *Biochemistry* 2014, 53, 7745−7754

in its denatured and reduced form.[25] However, the final yield of the recombinant protein after purification was too low to envision the resolution of its 3D structure by nuclear magnetic resonance (NMR). An alternative is to produce AhPDF1.1b by chemical means (see, for example, our previous work[26,27]). Chemical synthesis has never been used for the production of plant defensins, without doubt because of a rather long polypeptide backbone (~50 amino acids), the presence of a conserved cysteine at the C-terminus, which represents a synthetic challenge,[28] and the complexity of reaching the native cysteine pairing of four disulfide bridges.[29]

In this work, we report the first total chemical synthesis of a plant defensin, AhPDF1.1b, and its detailed NMR structural study in the overall context of other CS$\alpha\beta$ defensins. Because small variations in the primary structure and/or small conformational changes in the 3D structure could account for multiple biological activities, we focused on a fine 3D characterization of AhPDF1.1b to gain further insight into the structural requirement for the antifungal and zinc tolerance activities.

MATERIALS AND METHODS

Synthetic AhPDF1.1b Sequence. ZRLCE KPSGT WSGVC GNNGA CRNQC IRLEK ARHGS CNYVF PAHKC ICYFP C, Z being a pyroglutamic acid residue.

RP-HPLC and Mass Spectrometry (MS) Analyses. The peptides were analyzed by RP-HPLC (reverse-phase high-performance liquid chromatography) and MALDI-TOF (matrix-assisted laser desorption ionization time-of-flight) mass spectrometry. HPLC analyses were conducted either on a LaChrom Elite system equipped with a Hitachi L-2130 pump, a Hitachi L-2455 diode array detector, and a Hitachi L-2200 autosampler or on a LaChrom 7000 system equipped with a Merck-Hitachi L-7100 pump, a Merck-Hitachi L-7455 diode array detector, and a Merck-Hitachi D-7000 interface, which was also used for semipreparative purification. The machines were equipped with C18 reversed-phase columns (Nucleosil, 300 Å, 5 μm, 250 mm × 4.6 mm for the analytical separations, or 250 mm × 10.5 mm for purification). Solvents A and B were 0.1% trifluoroacetic acid (TFA) in H_2O and 0.1% TFA in MeCN, respectively. MS analyses were performed on an Ultraflex MALDI-TOF instrument (Bruker Daltonics, Bremen, Germany) equipped with a 337 nm nitrogen laser and a gridless delayed extraction ion source. The instrument was used in positive ion reflector mode with a 150 ns delay and an accelerating voltage of 19 kV. Instrument control and external calibration were accomplished using FLEXcontrol (Bruker). The observed m/z values correspond to the monoisotopic ions.

Peptide Synthesis. Solid-phase peptide synthesis (SPPS) was conducted on a 433A automated synthesizer from Applied Biosystems (Courtaboeuf, France) using Fmoc/*t*Bu chemistry on a 0.1 mmol scale with *O*-(6-chlorobenzotriazol-1-yl)-*N*,*N*,*N*′,*N*′-tetramethyluronium hexafluorophosphate (HCTU) as a coupling reagent in the presence of a 2-fold excess of iPr$_2$NEt in *N*-methylpyrrolidone (NMP). The elongation was conducted automatically from a H-Cys(Trt)-Trityl-ChemMatrix resin (loading of 0.31 mmol/g) (PCAS BioMatrix, St-Jean-sur-Richelieu, QC) using a 10-fold excess of protected amino acids and coupling reagents. Fmoc deprotection was performed using a 20% piperidine solution in NMP. Each coupling step was followed by capping with acetic anhydride. The following side chain protecting groups were used: Arg(Pbf), Asn(Trt), Cys(Trt), Glu(O*t*Bu), Gln(*t*Bu), His(Trt), Lys(Boc), Ser(*t*Bu), Thr(*t*Bu), Trp(Boc), and Tyr(*t*Bu). The 0.1 mmol scale program purchased from the manufacturer was used, modified by doubling the reaction volumes and coupling times to fit with the high swelling of the ChemMatrix resin. After completion of the peptide elongation, the peptide resin was transferred into a polypropylene syringe fitted with a polypropylene frit (Torviq, Niles, MI) and treated with a TFA/H_2O/iPr$_3$SiH/phenol mixture (88:5:2:5) for 3 h. After filtration, the peptide was precipitated by dilution into cold diethyl ether, recovered by centrifugation, and washed three times with diethyl ether. Then the pellet was dissolved in H_2O containing 0.1% TFA. The reduced form was purified by semipreparative C18 reverse-phase HPLC and lyophilized. Reduced synthetic AhPDF1.1b: MALDI-TOF $[M + H]^+$ m/z 5687.61 (calcd for $C_{242}H_{373}N_{76}O_{68}S_8$ m/z 5687.57); HPLC analytical gradient 20 to 40% B/A over 30 min; retention time 22.5 min.

Oxidative Folding. The oxidative folding experiments were conducted under argon at different pHs and temperatures on the reduced form of an HPLC-purified AhPDF1.1b solution (final concentration of 12 μM) in Tris-HCl buffer (final concentration of 100 mM), 1 mM ethylenediaminetetraacetic acid (EDTA), and a mixture of reduced (GSH) and oxidized glutathione (GSSG) at a peptide:GSH:GSSG molar ratio of 1:100:10. The peptide concentration was determined using UV spectrophotometry at 280 nm (ε_{red} = 8480 M^{-1} cm^{-1}; ε_{oxi} = 8980 M^{-1} cm^{-1}). The time course of oxidative folding was followed by taking aliquots from the reaction mixture, quenching the oxidation by acidifying the sample with TFA (final concentration of 2%), and then analyzing the sample by analytical HPLC (gradient from 20 to 40% B/A over 30 min, at a rate of 1 mL/min). The oxidative yield of AhPDF1.1b was calculated from integrated HPLC peak areas estimated at λ = 280 nm. The preparative scale oxidative folding of AhPDF1.1b was conducted under optimized folding conditions (45 °C and pH 8.5) over 4 h. After acidification with TFA (final concentration of 2%), the peptide was purified by semi-preparative C18 reverse-phase HPLC and lyophilized.

Oxidized synthetic AhPDF1.1b: MALDI-TOF $[M + H]^+$ m/z 5679.48 (calcd for $C_{242}H_{365}N_{76}O_{68}S_8$ m/z 5679.52); HPLC analytical gradient 20 to 40% B/A over 30 min; retention time 16.1 min.

Antifungal Assays. Growth inhibition assays were conducted against *Fusarium oxysporum* f. sp. *melonii* (given by INRA Avignon) as described previously.[25] The minimal inhibitory concentration (MIC) was determined as the lowest defensin concentration that induced 100% reduction of growth compared with the inhibitor-free growth conditions. Three biological repetitions were conducted for each defensin concentration.

NMR Spectroscopy. The synthetic peptide was dissolved in a 9:1 (v/v) H_2O/D_2O mixture, leading to a protein concentration of 1.3 mM. The final pH of the AhPDF1 solution, adjusted with minute increments of 1 N HCl, was 4.5. NMR spectra were recorded on a 600 MHz VARIAN INOVA NMR spectrometer equipped with a z-axis field-gradient unit. Standard VARIAN library pulse programs were acquired in phase-sensitive mode, with quadrature detection in both directions using the States method and WATERGATE water suppression. A standard set of two-dimensional ^{1}H NOESY (nuclear Overhauser enhancement spectroscopy) with a mixing time of 160 ms, TOCSY (total correlation spectroscopy) with an MLEV of 80 ms, and DQF-COSY (double-quantum-filtered correlation spectroscopy) NMR experiments were performed at

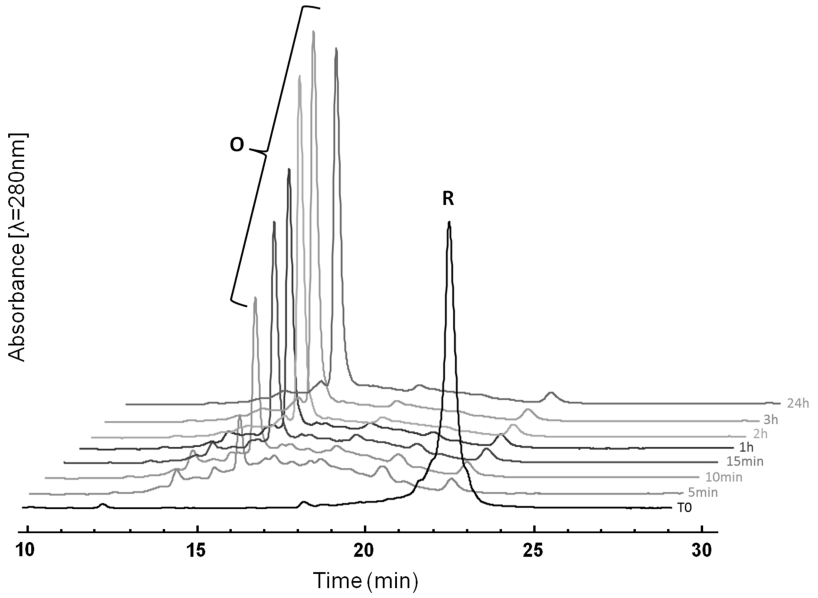

Figure 1. HPLC traces of AhPDF1.1b during oxidative folding. The reduced form of AhPDF1.1b (R) was folded in the presence of GSH and GSSG, at 45 °C, in 100 mM Tris buffer (pH 8.5) containing 1 mM EDTA to give the oxidized form of AhPDF1.1b (O). The reaction was quenched by acidification before being analyzed by C18 RP-HPLC [gradient from 20 to 40% B/A over 30 min (solvents A and B were 0.1% TFA in H_2O and 0.1% TFA in MeCN, respectively)]. The initial conditions (T0) correspond to the sample prior to the addition of the redox system.

298 and 308 K. Natural-abundance ^{13}C HSQC and fast ^{15}N HSQC spectra were recorded at 298 K with 700 FIDs and 63 scans (63 h) and 300 FIDs and 960 scans (94 h), respectively. ^{1}H chemical shifts were referenced to DSS used as an internal standard. ^{15}N and ^{13}C chemical shifts were indirectly referenced to DSS as described by Wishart et al.[30] Spectra were processed with NMRPIPE[31] and analyzed with CCPNMR (version 2.2.2).[32] DOSY experiments were performed on a 700 MHz Avance III instrument equipped with a cryoprobe using a standard Bruker sequence and diffusion protocol described in the NMR user manual. Calibration of the gradient strength was performed on a 99.9% D_2O/0.1% $GdCl_3$ sample at 25 °C.

Structure Calculations. Nuclear Overhauser effects (NOEs) were used to determine a set of empirical structural parameters, such as inter- and intraresidue distance restraints. Structures were performed with NOE distance by using CNS[33,34] incorporating automatic assignment software ARIA2 (version 2.3).[35] The pyroglutamic acid residue (PCA) located at the N-terminal position of the AhPDF1.1b sequence is considered as a nonstandard residue in CNS. Topology libraries (topalldg5.3.pro and topalldg5.3.pep) were modified as described in the ARIA 2.3 tutorials. Covalent bonds were added between sulfur atoms involved in each bridge (Cys4−Cys51, Cys15−Cys36, Cys21−Cys45, and Cys25−Cys47) by homology with all the other 3D structures of plant defensins and in accordance with intra-cysteine NOE connectivities [Cys4 (H_N)/Cys51 (H_N), Cys15 (Hβ)/Cys36 (Hα), Cys21 (Hβ)/Cys45 (Hα), and Cys25 (Hβ)/Cys47 (Hα)]. The ARIA2 protocol used simulated annealing with torsion angle and Cartesian space dynamics with the default parameters. The iterative process was repeated until the assignment of the NOESY map was complete. The last run, performed with 500 initial structures, used a list of 943 NOE-derived distance restraints. The final structures were displayed and analyzed using MOLMOL,[36] and their qualities were evaluated using PROCHECK-NMR and PROMOTIF.[37,38] The figures were drawn with PYMOL[39] and MOLMOL.[36]

Comparative Modeling. Comparative modeling, or homology modeling, was performed with MODELER,[40] taking AhPDF1.1b as the template, to build the 3D structures of all AtPDF1 and AhPDF1 defensins with known sequences, except for the truncated AhPDF1.7 defensin. Multiple-sequence alignments were performed using the online Clustal Omega (EMBL-EBI Website). Molecular surfaces were created, and surface properties (hydrophobic and electrostatic potentials) were analyzed with MOE (Molecular Operating Environment, Chemical Computing Group, Montreal, QC).

RESULTS

Synthesis and Chemical Characterization of Oxidized Synthetic AhPDF1.1b. The AhPDF1.1b sequence, deduced from the gene,[41] includes an N-terminal glutamine,[25] a residue that is well-known for being able to spontaneously cyclize into a pyroglutamyl residue. We observed such a spontaneous cyclization during preliminary oxidative folding experiments conducted with recombinant AhPDF1.1b, and we decided to introduce an N-terminal pyroglutamyl residue that we hypothesize to be present in the natural AhPDF1.1b. In support of this hypothesis, the RsAFP1 defensin isolated from *R. sativus* seeds, being 90% identical to AhPDF1.1b, contains an N-terminal pyroglutamyl residue.[9]

The peptide elongation of AhPDF1.1b was conducted by SPPS following the Fmoc/*t*Bu strategy using a polar resin facilitating the synthesis of "difficult sequences" and long peptides[42,43] and a 2-chlorotrityl resin to minimize the epimerization of the C-terminal Cys residue.[44] After completion of the elongation and TFA treatment, the reduced form of AhPDF1.1b was precipitated by dilution into cold diethyl ether. Analysis by HPLC and mass spectrometry revealed that the major peak was accompanied by a smaller one corresponding to the same mass (Figure S1 of the Supporting Information). This was attributed to an epimerization during the 51 repetitive piperidine treatments (i.e., 8 h).[45,46] Minor peaks with ΔM values of +56 and +51 Da were also observed

dx.doi.org/10.1021/bi501285k | *Biochemistry* 2014, 53, 7745−7754

and attributed to the well-known *tert*-butyl group adducts produced during the TFA treatment and to the C-terminal 3-(1-piperidinyl) alanine formation,[28] respectively. Other minor peaks were characterized as acetylated truncated peptides. After purification of the reduced form of AhPDF1.1b by HPLC (Figure S2 of the Supporting Information), the oxidative folding was optimized using a procedure based on a thermodynamically controlled disulfide shuffling, in the presence of reduced and oxidized glutathione (Figure 1). The folding kinetics was followed by quantitative analytical HPLC. Different pH and temperature combinations were screened, and pH 8.5 and 45 °C, the best conditions tested, proved to be perfectly satisfactory in terms of conversion yield (Figure S3 of the Supporting Information) and were selected for preparative scale oxidative folding. MALDI-TOF MS analysis of oxidized AhPDF1.1b showed a −8 Da difference in mass compared to that of the reduced form, consistent with the fully oxidized form of the peptide (Figure S4 of the Supporting Information). AhPDF1.1b was produced in a 4% satisfactory yield (starting from the initial resin substitution), considering the challenging sequence.

Antifungal Activity of the Synthetic AhPDF1.1b. The synthetic AhPDF1.1b defensin was assayed *in vitro* for its ability to inhibit the growth of *F. oxysporum* f. sp. *melonii*. It showed a minimal inhibitory concentration (MIC) of 2 μM (Figure 2 and Figure S5A of the Supporting Information). This value is similar to the MIC previously found for the recombinant AhPDF1.1b (2.5 μM) (Figure S5B of the Supporting Information).[41]

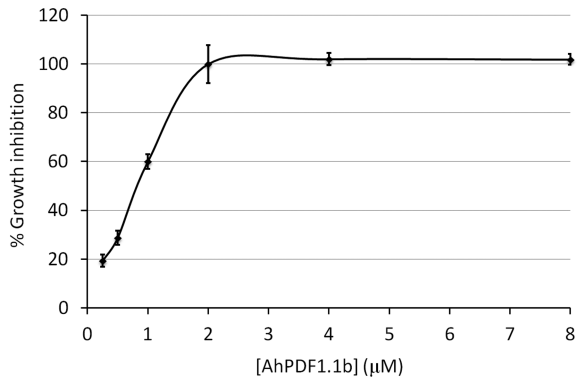

Figure 2. Antifungal activity of synthetic AhPDF1.1b. Growth inhibition of *F. oxysporum* sp. *melonii* was measured in the presence of increasing AhPDF1.1b concentrations to estimate the minimal inhibitory concentration (MIC) for the synthetic defensin. Error bars correspond to standard errors; n = 3 biological repetitions.

AhPDF1.1b Adopts a Typical CS$\alpha\beta$ Fold. The 3D structure of AhPDF1.1b was determined by NMR spectroscopy. The one-dimensional ^{1}H NMR spectrum showed good dispersion (≈4 ppm) in the amide region, indicative of a highly structured peptide. Two-dimensional ^{1}H NMR spectra allowed a complete assignment of ^{1}H chemical shifts (BRMB entry 19237). Natural-abundance heteronuclear NMR spectra allowed 25 N_H, 35 Cα, and 31 Cβ shifts to be assigned along with many side chain carbon chemical shifts. This helped us to unambiguously assign ^{1}H chemical shifts, particularly in crowded regions of the ^{1}H NOESY spectra corresponding to side chains. As some plant defensins were reported as dimers,[15,17] it was important to define the oligomeric state of AhPDF1.1b before structure calculation. Determination of the translational diffusion coefficient from pulsed field gradient NMR experiments allowed us to estimate that the peptide mass is 5000 ± 400 Da, which is compatible with a monomeric form of our NMR sample of AhPDF1.1b (Figure S6 of the Supporting Information).

The Phe40−Pro41 amide bond predominantly adopts an unusual *cis* conformation as shown by the observed NOEs: Phe40 (Hα)/Pro41 (Hα) and Phe40 (HN)/Pro41 (Hα). A minor *trans* conformer (15%) of Pro41 was observed in NOESY spectra of AhPDF1.1b. Therefore, Pro41 was set to be *cis* in the ARIA2 protocol.

The 3D structure of AhPDF1.1b was calculated by taking into account a total of 943 distance restraints (Table 1). The number of NOE restraints was sufficient to reach a good convergence in the calculation. Therefore, neither dihedral constraints nor H bond constraints were added. Among the 50 best refined structures, 10 structures were selected, in agreement with all of the experimental data and the standard covalent geometry. They were considered as being representative of the solution structure of AhPDF1.1b. Coordinates were deposited as PDB entry 2M8B.

Table 1. Experimental Restraints and Structural Statistics of AhPDF1.1b[a]

NMR Constraints		
distance restraints		
total NOE	943	
unambiguous	859	
ambiguous	84	
Structural Statistics for the Ensemble of the 10 Lowest-Energy Structures		
	backbone atoms	heavy atoms
average pairwise root-mean-square deviation (rmsd) (Å)		
residues 2−51	0.68 ± 0.12	1.51 ± 0.33
average rmsd[b](Å)		
helix α (residues 18−27)	0.50 ± 0.12	1.26 ± 0.30
strand β1 (residues 4−7)	0.45 ± 0.15	1.18 ± 0.47
strand β2 (residues 32−39)	0.48 ± 0.12	1.03 ± 0.19
strand β3 (residues 42−49)	0.45 ± 0.13	0.72 ± 0.14
β1−α loop (residues 8−17)	0.89 ± 0.27	1.20 ± 0.28
α−β2 loop (residues 28−31)	0.48 ± 0.16	1.02 ± 0.25
β2−β3 loop (residues 40 and 41)	0.99 ± 0.41	1.31 ± 0.51
average violations per structure		
NOEs ≥0.5 Å	0	
NOEs ≥0.3 Å	0.1	
Ramachandran analysis (%)		
most favored region	85.85	
allowed region	14.15	
generously allowed	0	
disallowed	0	

[a]Structural statistics are calculated for the ensemble of the ten lowest-energy structures. [b]Average rmsd are calculated after fitting the secondary structure elements (α1, β1-3) as is on Figure 4A.

AhPDF1.1b displays the typical CS$\alpha\beta$ fold of the plant defensins (Figure 3). Analysis of the 10 final structures with PROCHECK-NMR[37] showed that all the residues were in the most favored (85.9%) or additionally allowed (14.1%) regions of the Ramachandran diagram (Table 1). Analysis of the structures with PROMOTIF[38] identified one α-helix between residues 18 and 27 and one β-sheet consisting of three antiparallel strands between residues 4 and 7, 32 and 39, and 42 and 49. A long loop of 10 residues (β1−α loop, residues 8−17)

dx.doi.org/10.1021/bi501285k | *Biochemistry* 2014, 53, 7745−7754

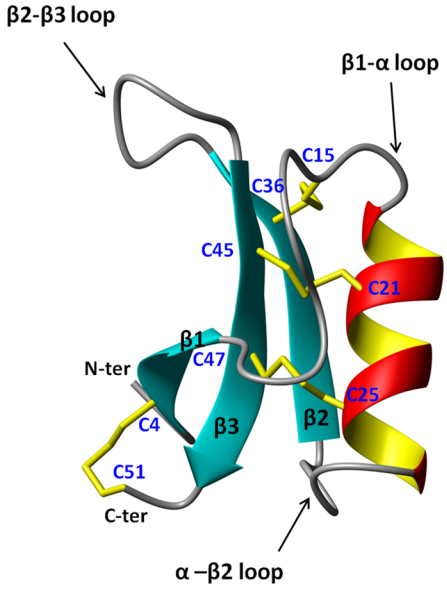

Figure 3. Schematic representation of the AhPDF1.1b backbone, which adopts the typical CS$\alpha\beta$ fold (drawn with MOLMOL[36]). The three strands of the β-sheet (cyan) are numbered from the N- to C-terminus (β1 to β3), and cysteine residues are numbered to clearly identify the disulfide bridges (colored yellow). The α-helix is colored red and yellow.

links strand β1 to the α-helix, with a type I β-turn around Ser8-Gly9-Thr10-Trp11. A shorter $\alpha-\beta$2 loop (residues 28–31) is structured with a type I β-turn around Arg27-Leu28-Glu29-Lys30. Finally, the β2–β3 loop involving Val39-Phe40-Pro41-Ala42 residues is structured with a dominant type VIa1 β-turn. The superimposition of the 10 models of AhPDF1.1b (Figure 4A) shows that the peptide is globular and compact. The rmsd calculated on secondary structure elements is 0.47 ± 0.13 Å. Only the β1–α loop and the β2–β3 loop show a greater mobility, with backbone rmsd values of 0.89 ± 0.27 and 0.99 ± 0.41 Å, respectively (Table 1).

It is commonly accepted that antimicrobial activities of AMPs require a subtle balance between cationicity and hydrophobicity. In AhPDF1.1b, the face corresponding to the helix is globally positive; β1–α and β2–β3 loops create hydrophobic patches at the top of the molecule, whereas cationic and hydrophobic residues are scattered on the surface (Figure 4B,C). Thus, overall, AhPDF1.1b contains cationic and hydrophobic residues exposed at the surface but lacks amphipathic architecture.

Homology Modeling of the Forms of PDF1 from *A. halleri* and *Arabidopsis thaliana*. Peptide sequences for forms of AhPDF1 from *A. halleri* and AtPDF1 from *A. thaliana* have been previously predicted from *PDF1* genes.[41] Some of them differ only in their N-terminal secretory signal peptide but lead to the same mature form (AtPDF1.2a, AtPDF1.2b, and AtPDF1.2c). For the 18 available Ah- and AtPDF1 sequences (Figure 5), the 3D structures were built by homology modeling using the experimental AhPDF1.1b structure as a target. As expected, the 3D folds can be superimposed on the target structure. Surface properties (hydrophilic/hydrophobic and electrostatic) were calculated for the ensemble of Ah- and AtPDF1 structures to gain insight into structure–activity

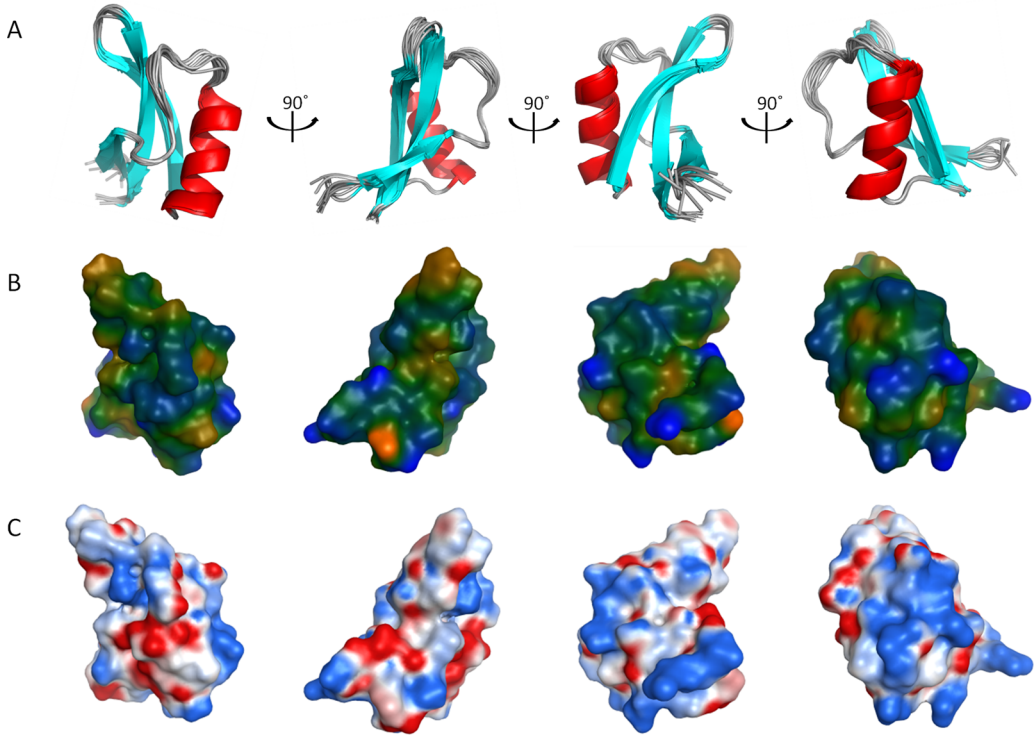

Figure 4. Surface properties of AhDPF1.1b, with a 90° rotation from left to right. (A) Superimposition of the 10 NMR structures of AhPDF1.1b drawn with PYMOL[39] (α-helix colored red, β-strands cyan, and loops and turns gray). (B) Hydrophobic and hydrophilic potential areas, calculated with the MOE software at the Connolly surfaces, are colored brown and blue, respectively. Green surfaces represent an intermediate hydrophobicity (symmetric scale). (C) Electrostatic positive and negative areas, calculated with MOE software based on the solution to the Poisson–Boltzmann equation, are colored blue and red, respectively (scale from −40 to 40 eV).

dx.doi.org/10.1021/bi501285k | *Biochemistry* 2014, 53, 7745–7754

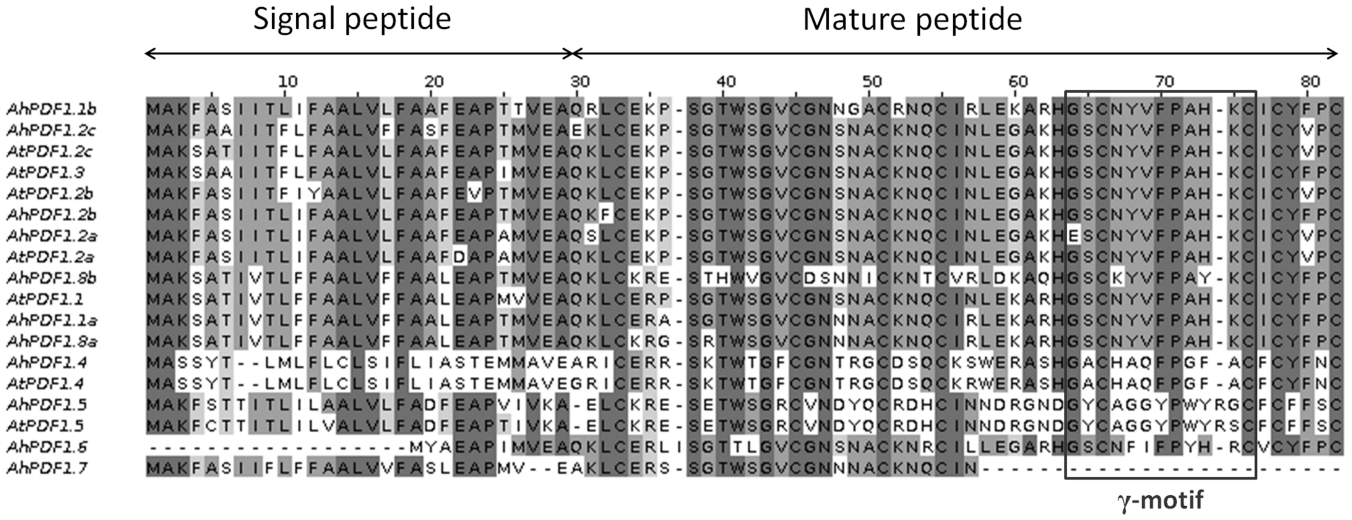

Figure 5. Comparative sequence alignment of predicted amino acid sequences encoded by *PDF1* genes from *A. halleri* and *A. thaliana*. The signal and mature peptide sequences and the γ-motif are specified.

relationships. All of the forms of PDF1 are cationic except AhPDF1.5 and AtPDF1.5, which present anionic surfaces (Figure S7 of the Supporting Information). For the others, cationic and hydrophobic residues are scattered on the surface, but none of them displays amphipatic properties, even for defensins showing weak sequence identity with AhPDF1.1b. Some defensins differing by only a few residues display significant modifications of biological activities. For example, AhPDF1.4 from *A. halleri* and AtPDF1.4 from *A. thaliana* differ by only two residues (Ala1 and Gly1 and Ser27 and Arg27, respectively), leading to subtle observable changes in the calculated surface properties (Figure 6).[41]

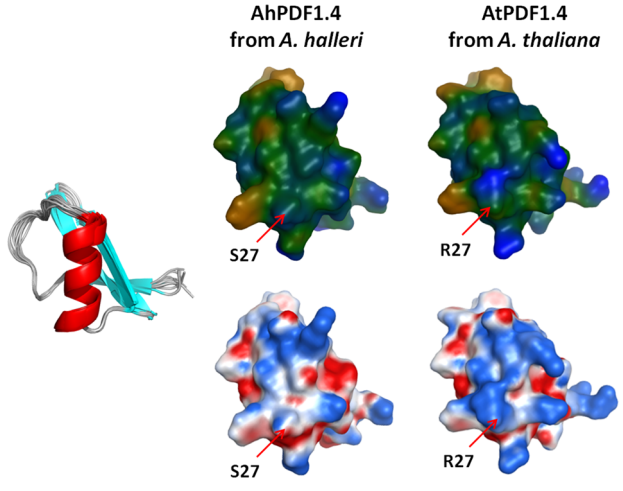

Figure 6. Surface properties of AhDPF1.4 and AtPDF1.4 showing S27 and R27, respectively. The top structures show hydrophobic and hydrophilic potential areas, calculated with the MOE software at the Connolly surfaces, colored brown and blue, respectively. Green surfaces represent an intermediate hydrophobicity (symmetric scale). The bottom structures show electrostatic positive and negative areas, calculated with MOE software based on the solution to the Poisson–Boltzmann equation, colored blue and red, respectively (scale from −40 to 40 eV). The left structure shows the orientation of the molecules.

DISCUSSION

All the 3D structures of plant defensins currently determined display a conserved CSαβ fold.[47] However, some defensins display a comparable spectrum of activities despite low levels of sequence homology, whereas other defensins with highly homologous sequences differ in one or several activities (Figure 7). It is then tricky to relate the function(s) to the sequence or structure. Moreover, the identification of functional areas from the distribution of cationic and hydrophobic residues scattered on the surface is not obvious. Small conformational changes in the 3D structure and/or subtle variations in surface properties could account for divergent or additional functions. To gain initial insights into the structural requirement for multifunctional plant defensins, we have combined our fine 3D characterization of AhPDF1.1b with a large set of 3D structures, and previous biological data for two activities, antifungal properties and ability to tolerate zinc.

Structural Features of Plant Antifungal CSαβ Defensins. Most of the roles described for plant defensins are due to specific interactions with plasma membrane components.[48] Thevissen et al. proposed that glycosylceramides present in the fungus membrane are the main receptors for plant defensin binding.[49] Moreover, several structure–activity studies indicate that the major determinants of antifungal activity reside in the γ-core motif[50] (Figure 7). For example, variations in the essential γ-core motif of MsDef1 and MtDef4 are responsible for the differences in antifungal spectra and morphological response in the fungus.[51] The γ-core motif was also highlighted as being functionally important in DmAMP1, which binds to mannose diinositolphosphoceramide (MI_2PC).[52] Recently, a novel cell lysis mechanism for fungal and tumor cells was described for NaD1 that acts via direct binding to the plasma membrane phospholipids, including phosphatidylinositol 4,5-biphosphate (PIP2).[53] In the crystal structure of a NaD1:PIP_2 complex (PDB entry 4CQK), seven dimers of NaD1 cooperatively bind the anionic headgroups of 14 PIP_2 molecules through a unique "cationic grip". This lipid binding grip belongs to the β2–β3 loop within the γ-motif.

The γ-core motif is a molecular signature of the plant defensins, but several structure–activity studies highlight the importance of dynamics of the β1–α and α–β2 loops. Thus,

dx.doi.org/10.1021/bi501285k | *Biochemistry* 2014, 53, 7745–7754

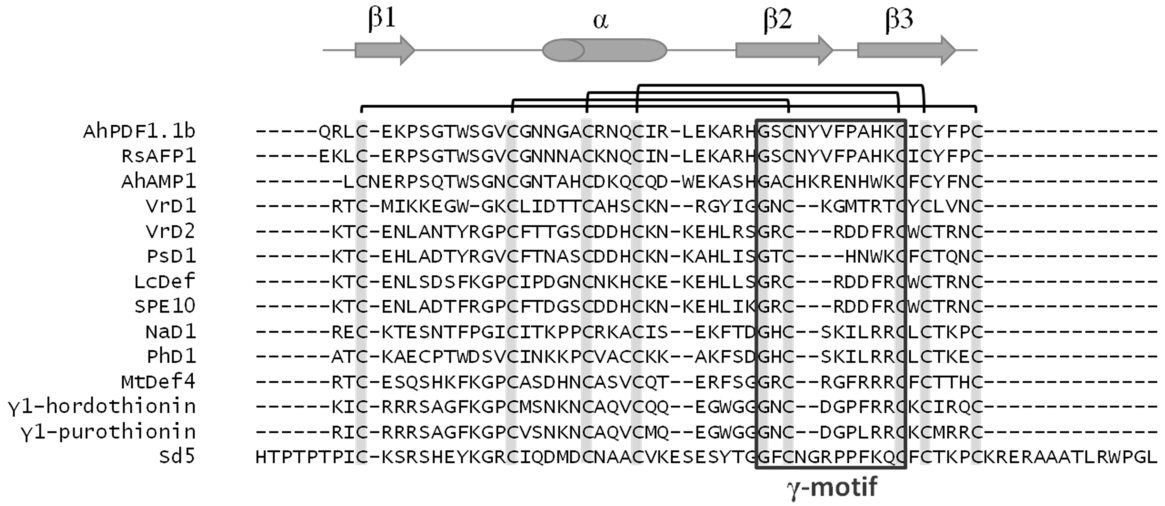

Figure 7. Alignment of the 14 sequences of plant defensins for which the 3D structure was determined. The γ-core motif, the four disulfide bridges, and the secondary structure elements are highlighted.

specific residues, essential for antifungal activity, conserved or not in AhPDF1.1b, were pointed out. (i) In the case of RsAFP2, 10 amino acids belonging to the $\beta1-\alpha$ and $\alpha-\beta2$ loops and the γ-core motif were identified as being essential for antifungal activity[54,55] and are conserved in AhPDF1.1b. Thus, we can postulate a similar role of these residues. (ii) For Psd1, the $\beta1-\alpha$ loop and the $\beta2-\beta3$ loop belonging to the γ-core motif were mapped as binding sites using mimetic systems of the *Fusarium solani* membrane,[56] but the Phe15 and Thr16 residues shown to be responsible for the specific interaction of Psd1 with glucosylceramide are never conserved in Ah- or AtPDF. (iii) Finally, in the case of the sugar cane Sd5 defensin, the $\alpha-\beta2$ loop is proposed to be responsible for the interaction with glucosylceramide,[19] but the involved residues are absent from Ah- and AtPDF. In summary, the precise mechanisms on the atomic scale are not yet clearly understood, and the great divergence in primary structure hampers the easy identification of a unique binding site (Figure 7).

***cis*–*trans* Conformation of Pro in the γ-Core Motif of CSαβ Proteins.** *cis*–*trans* isomerization of amide bonds is known to play critical roles in protein molecular recognition, protein folding, protein misfolding, and diseases.[57] In AhPDF1.1b, a Pro residue is present in the γ-core motif, and the Phe40–Pro41 amide bond predominantly adopts an unusual *cis* conformation. In the Protein Data Bank, 56 3D structures of proteins exhibiting a CSαβ motif are available: 14 plant defensins (AhPDF1.1b included), six insect defensins, four fungus defensins, one mussel defensin, and 31 scorpion toxins. Among them, only 10 proteins possess one (sometimes two) Pro residue(s) located in the γ-core motif (Figure 8). In addition to AhPDF1.1b, *cis*-Pro was observed in NMR structures of only two other plant defensins, RsAFP1 and Sd5, and in the crystal 3D structures of the scorpion toxin Ts1 (Figure 8). Conversely, for six other CSαβ proteins, the Gly/Ser–Pro amide bonds located in the γ-motif adopt a *trans* conformation.

The type VI turn is the unique member of the β-turn family that incorporates a *cis* prolyl bond, and the four consecutive residues (Val39-Phe40-Pro41-Ala42) present in AhPDF1.1b are known to strongly favor a VIa1 β-turn conformation around the *cis*-Pro.[58] Indeed, the presence of an aromatic residue such as Phe40 (position $i+1$) preceding Pro is essential. Moreover,

Plant	AhPDF1.1b	2M8B	GSCNYVF**P**--AHK--C
	RsAFP1	1AYJ	GSCNYVF**P**--AHK--C
	Sd5	2KSK	GFCNGR**P**P--FKQ--C
	γ1-Hordothionin	1GPS	GNC--DG**P**--FRR--C
	γ1-Purothionin	1GPT	GNC--DG**P**--LRR--C
Fungus	Micasin	2LR5	GFC--AG**P**--LRA-TC
	Eurocin	2LT8	GYC--AG**P**WYLGH**P**TC
Insect	Drosomycin	1MYN	GHC---S**P**-SLK---C
Scorpion	Toxin II	1PTX	GYCQWAS**P**-YGNA--C
	Toxin Ts1	1NPI	GYC--AW**P**--A----C

Figure 8. Sequence alignment of the γ-core motif of CSαβ proteins, from various origins, possessing at least one Pro residue in this region. Conserved Gly and Cys residues are colored light and dark gray, respectively. *cis*-Pro residues are highlighted in black and *trans*-Pro residues in bold.

a β-branched residue like Val39 (residue i) and Ala42 (position $i+3$) stabilize this *cis* conformation.[58] The tetrapeptide (Val-Phe-Pro-Ala) is conserved in 12 of 17 types of Ah- and AtPDF1 (Figure 5). Pro is preceded by an aromatic residue (Phe/Tyr) in all of them except for the truncated AhPDF1.7 lacking the 24 C-terminal residues.[41] Moreover, the Phe-Pro dipeptide is conserved in all *Arabidopsis lyrata* defensins.[41] Thus, this *cis*-Pro residue, favored by neighboring residues, is doubtless a key for one or several functions.

For another class of plant AMPs, the Möbius cyclotides,[59] the *cis*-Pro conformation has been reported as being essential for binding to the target membrane. These cystine knot peptides are involved in multiple functions, all related to their strong interaction with membranes. For example, Kalata B1 is antibacterial, insecticidal, molluscicidal, nematocidal, anti-HIV, and hemolytic.[60] In this case, Trp23 and *cis*-Pro24 insert into lipid bilayers to form membrane pores destabilizing the membrane through hydrophobic and phosphoethanolamine-specific interactions.[61]

Evolvability of Plant Defensins. Comparison of potential surfaces of PDF1 defensins could not evidence patterns of charge distribution or hydrophobic/hydrophilic patches among the ensemble of proteins, which could easily correlate surface properties to biological activities. Moreover, slight changes in the sequence cannot be correlated with significant variation of activity. For example, it is tricky to explain why AtPDF1.4 from *A. thaliana*, differing from AhPDF1.4 from *A. halleri* by only

dx.doi.org/10.1021/bi501285k | *Biochemistry* 2014, 53, 7745–7754

two residues, confers more zinc tolerance. Evolvability defines the ability of proteins to adopt new functions within existing (or even new) folds.[62] In the case of rigid structures, such as the CS$\alpha\beta$ proteins, this evolvability could originate from movements of loops.[62] We focused on the $\beta2-\beta3$ loop containing the *cis*-Pro41 (AhPDF1.1b numbering). Because this Pro is not a conserved residue for CS$\alpha\beta$ proteins, it is not essential for the 3D fold itself. Moreover, Pro41 is not conserved in antifungal plant defensins; therefore, it is not essential for the antifungal activity but could be related to zinc tolerance.

The ability to confer zinc tolerance in yeast has been previously reported for 18 types of *Arabidopsis* PDF1 along with the antifungal activity for 11 of them.[41] As shown in Figure 9, all 12 forms of PDF1 that confer a high zinc tolerance harbor

PDF1	γ-motif	zinc tolerance
AhPDF1.1a *AhPDF1.1b* *AhPDF1.2a* *AhPDF1.2b* *AhPDF1.2c* *AhPDF1.8a* *AhPDF1.8b* AtPDF1.1 AtPDF1.2a AtPDF1.2b AtPDF1.2c AtPDF1.3	XXCXX**VFPA**XXXC	++
AhPDF1.4 AtPDF1.4	XXCXX**QFPG**XXXC	– +
AhPDF1.5 AtPDF1.5	XXCXX**GYPW**XXXC	–

Figure 9. Comparative sequence alignment of the γ-core motif belonging to *A. halleri* and *A. thaliana PDF1* defensins and their ability to confer zinc tolerance in yeast (adapted from ref 41).

the Val-Phe-Pro-Ala sequence containing the presumed *cis*-Pro conformation in their γ-motif. Among them, the forms of *A. halleri* PDF1 that have been produced and tested for their antifungal activity also showed good antifungal activity against *F. oxysporum* sp. *melonii*, except AhPDF1.8b.[41] The case of AhPDF1.8b is singular as its mature peptide sequence significantly differs from those of other forms of AhPDF1, whereas the Val-Phe-Pro-Ala sequence is fully conserved (Figure 5). At the functional level, its antifungal activity is very low[41] whereas its zinc tolerance activity is fully efficient. Remarkably, when the Val-Phe-Pro-Ala sequence is not strictly conserved, zinc tolerance activity decreases as for AtPDF1.4 and even collapses as for AhPDF1.4, AhPDF1.5, and AtPDF1.5 (Figure 9). It thus turns out that for all the forms of *Arabidopsis* PDF1 for which the ability to confer zinc tolerance has been established, the Val-Phe-Pro-Ala sequence containing the presumed *cis*-Pro conformation is fully conserved and its alteration deeply impairs the function.

As structural and/or dynamic modification of loops can lead to evolvability,[62] we hypothesized that *cis*-Pro isomerism and/or *cis*–*trans* isomerization certainly ensures structural or dynamic features essential for zinc tolerance activity. Isomerization would impact the redox potential of the neighboring disulfide bonds and consequently zinc chelation.[63,64]

CONCLUSION

The γ-core motif conserved in all plant defensins is known to be involved in antifungal activity. We established here that the four consecutive residues (Val39-Phe40-Pro41-Ala42) present in AhPDF1.1b, which contain a *cis* amide bond and form a type VIa1 β-turn within this γ-core, are essential for zinc tolerance. On the basis of a set of structural and functional data for *A. halleri* and *A. thaliana* defensins, we demonstrated that if this sequence is not strictly conserved, zinc tolerance activity decreases and even collapses. The $\beta2-\beta3$ loop sequence (Val-Phe-Pro-Ala) within the γ-core would ensure structural or dynamic features essential for the chelation of zinc. Our hypothesis is that the zinc tolerance capacity of AhPDF1.1b would rely on the oxidative state of cysteines. The *cis* conformation of the Phe40–Pro41 bond within this β-turn or its *cis*–*trans* isomerization could impact the redox potential of the two neighboring disulfide bridges allowing zinc chelation.

ASSOCIATED CONTENT

Supporting Information

Supplementary Figures S1–S7. This material is available free of charge via the Internet at http://pubs.acs.org.

Accession Codes

Coordinates have been deposited in the PDB as entry 2M8B, and chemical shifts were deposited in the BioMagResBank as entry 19237.

AUTHOR INFORMATION

Corresponding Author

*E-mail: francoise.paquet@cnrs-orleans.fr. Phone: +33 238 257692.

Funding

F.M. was supported by a doctoral fellowship from the CNRS and Région Centre.

Notes

The authors declare no competing financial interest.

ACKNOWLEDGMENTS

We thank Hervé Meudal (Centre de Biophysique Moléculaire, Orléans, France) for technical assistance with NMR spectrometers, Philippe Marceau (Centre de Biophysique Moléculaire) for HPLC, and the mass spectrometry facilities of CBM.

REFERENCES

(1) Aerts, A. M., Francois, I. E., Cammue, B. P., and Thevissen, K. (2008) The mode of antifungal action of plant, insect and human defensins. *Cell. Mol. Life Sci. 65*, 2069–2079.

(2) Lacerda, A. F., Vasconcelos, E. A., Pelegrini, P. B., and Grossi de Sa, M. F. (2014) Antifungal defensins and their role in plant defense. *Front. Microbiol. 5*, 116.

(3) Meira Ribeiro, S., Farias Porto, W., Nascimento Silva, O., de Oliveira Santos, M., Campos Dias, S., and Luiz Franco, O. (2013) Plant Antifungal Peptides. In *Handbook of Biologically Active Peptides* (Kastin, A. J., Ed.) 2nd ed., pp 169–179, Elsevier Inc., Amsterdam.

(4) Cornet, B., Bonmatin, J. M., Hetru, C., Hoffmann, J. A., Ptak, M., and Vovelle, F. (1995) Refined three-dimensional solution structure of insect defensin A. *Structure 3*, 435–448.

(5) Landon, C., Pajon, A., Vovelle, F., and Sodano, P. (2000) The active site of drosomycin, a small insect antifungal protein, delineated by comparison with the modeled structure of Rs-AFP2, a plant antifungal protein. *J. Pept. Res. 56*, 231–238.

(6) Gachomo, E. W., Jimenez-Lopez, J. C., Kayode, A. P., Baba-Moussa, L., and Kotchoni, S. O. (2012) Structural characterization of plant defensin protein superfamily. *Mol. Biol. Rep. 39*, 4461–4469.

(7) Wilmes, M., Cammue, B. P., Sahl, H. G., and Thevissen, K. (2011) Antibiotic activities of host defense peptides: More to it than lipid bilayer perturbation. *Nat. Prod. Rep. 28*, 1350–1358.

(8) Bruix, M., Jimenez, M. A., Santoro, J., Gonzalez, C., Colilla, F. J., Mendez, E., and Rico, M. (1993) Solution structure of γ 1-H and γ 1-P thionins from barley and wheat endosperm determined by ^{1}H-NMR: A structural motif common to toxic arthropod proteins. *Biochemistry 32*, 715−724.
(9) Fant, F., Vranken, W., Broekaert, W., and Borremans, F. (1998) Determination of the three-dimensional solution structure of *Raphanus sativus* antifungal protein 1 by ^{1}H NMR. *J. Mol. Biol. 279*, 257−270.
(10) Fant, F., Vranken, W. F., and Borremans, F. A. (1999) The three-dimensional solution structure of *Aesculus hippocastanum* antimicrobial protein 1 determined by ^{1}H nuclear magnetic resonance. *Proteins 37*, 388−403.
(11) Almeida, M. S., Cabral, K. M., Kurtenbach, E., Almeida, F. C., and Valente, A. P. (2002) Solution structure of *Pisum sativum* defensin 1 by high resolution NMR: Plant defensins, identical backbone with different mechanisms of action. *J. Mol. Biol. 315*, 749−757.
(12) Lin, K. F., Lee, T. R., Tsai, P. H., Hsu, M. P., Chen, C. S., and Lyu, P. C. (2007) Structure-based protein engineering for α-amylase inhibitory activity of plant defensin. *Proteins 68*, 530−540.
(13) Liu, Y. J., Cheng, C. S., Lai, S. M., Hsu, M. P., Chen, C. S., and Lyu, P. C. (2006) Solution structure of the plant defensin VrD1 from mung bean and its possible role in insecticidal activity against bruchids. *Proteins 63*, 777−786.
(14) Lay, F. T., Brugliera, F., and Anderson, M. A. (2003) Isolation and properties of floral defensins from ornamental tobacco and petunia. *Plant Physiol. 131*, 1283−1293.
(15) Lay, F. T., Mills, G. D., Poon, I. K., Cowieson, N. P., Kirby, N., Baxter, A. A., van der Weerden, N. L., Dogovski, C., Perugini, M. A., Anderson, M. A., Kvansakul, M., and Hulett, M. D. (2012) Dimerization of plant defensin NaD1 enhances its antifungal activity. *J. Biol. Chem. 287*, 19961−19972.
(16) Janssen, B. J., Schirra, H. J., Lay, F. T., Anderson, M. A., and Craik, D. J. (2003) Structure of *Petunia hybrida* defensin 1, a novel plant defensin with five disulfide bonds. *Biochemistry 42*, 8214−8222.
(17) Song, X., Zhang, M., Zhou, Z., and Gong, W. (2011) Ultra-high resolution crystal structure of a dimeric defensin SPE10. *FEBS Lett. 585*, 300−306.
(18) Sagaram, U. S., El-Mounadi, K., Buchko, G. W., Berg, H. R., Kaur, J., Pandurangi, R. S., Smith, T. J., and Shah, D. M. (2013) Structural and functional studies of a phosphatidic acid-binding antifungal plant defensin MtDef4: Identification of an RGFRRR motif governing fungal cell entry. *PLoS One 8*, e82485.
(19) de Paula, V. S., Razzera, G., Barreto-Bergter, E., Almeida, F. C., and Valente, A. P. (2011) Portrayal of complex dynamic properties of sugarcane defensin 5 by NMR: Multiple motions associated with membrane interaction. *Structure 19*, 26−36.
(20) Yount, N. Y., and Yeaman, M. R. (2004) Multidimensional signatures in antimicrobial peptides. *Proc. Natl. Acad. Sci. U.S.A. 101*, 7363−7368.
(21) Carvalho, A. O., and Gomes, V. M. (2009) Plant defensins: Prospects for the biological functions and biotechnological properties. *Peptides 30*, 1007−1020.
(22) Huang, G. J., Lai, H. C., Chang, Y. S., Sheu, M. J., Lu, T. L., Huang, S. S., and Lin, Y. H. (2008) Antimicrobial, dehydroascorbate reductase, and monodehydroascorbate reductase activities of defensin from sweet potato [*Ipomoea batatas* (L.) Lam. 'Tainong 57'] storage roots. *J. Agric. Food Chem. 56*, 2989−2995.
(23) Hegedus, N., and Marx, F. (2013) Antifungal proteins: More than antimicrobials? *Fungal Biology Reviews 26*, 132−145.
(24) Mirouze, M., Sels, J., Richard, O., Czernic, P., Loubet, S., Jacquier, A., Francois, I. E., Cammue, B. P., Lebrun, M., Berthomieu, P., and Marques, L. (2006) A putative novel role for plant defensins: A defensin from the zinc hyper-accumulating plant, *Arabidopsis halleri*, confers zinc tolerance. *Plant J. 47*, 329−342.
(25) Marques, L., Oomen, R. J., Aumelas, A., Le Jean, M., and Berthomieu, P. (2009) Production of an *Arabidopsis halleri* foliar defensin in *Escherichia coli*. *J. Appl. Microbiol. 106*, 1640−1648.
(26) Derache, C., Meudal, H., Aucagne, V., Mark, K. J., Cadene, M., Delmas, A. F., Lalmanach, A. C., and Landon, C. (2012) Initial insights into structure-activity relationships of avian defensins. *J. Biol. Chem. 287*, 7746−7755.
(27) Herve, V., Meudal, H., Labas, V., Rehault-Godbert, S., Gautron, J., Berges, M., Guyot, N., Delmas, A. F., Nys, Y., and Landon, C. (2014) Three-dimensional NMR structure of hen egg gallin (chicken ovodefensin) reveals a new variation of the β-defensin fold. *J. Biol. Chem. 289*, 7211−7220.
(28) Lukszo, J., Patterson, D., Albericio, F., and Kates, S. (1996) 3-(1-Piperidinyl)alanine formation during the preparation of C-terminal cysteine peptides with the Fmoc/t-Bu strategy. *Lett. Pept. Sci. 3*, 157−166.
(29) Vriens, K., Cammue, B. P., and Thevissen, K. (2014) Antifungal plant defensins: Mechanisms of action and production. *Molecules 19*, 12280−12303.
(30) Wishart, D. S., Bigam, C. G., Holm, A., Hodges, R. S., and Sykes, B. D. (1995) ^{1}H, ^{13}C and ^{15}N random coil NMR chemical shifts of the common amino acids. I. Investigations of nearest-neighbor effects. *J. Biomol. NMR 5*, 67−81.
(31) Delaglio, F., Grzesiek, S., Vuister, G. W., Zhu, G., Pfeifer, J., and Bax, A. (1995) NMRPipe: A multidimensional spectral processing system based on UNIX pipes. *J. Biomol. NMR 6*, 277−293.
(32) Vranken, W. F., Boucher, W., Stevens, T. J., Fogh, R. H., Pajon, A., Llinas, M., Ulrich, E. L., Markley, J. L., Ionides, J., and Laue, E. D. (2005) The CCPN data model for NMR spectroscopy: Development of a software pipeline. *Proteins 59*, 687−696.
(33) Brunger, A. T., Adams, P. D., Clore, G. M., DeLano, W. L., Gros, P., Grosse-Kunstleve, R. W., Jiang, J. S., Kuszewski, J., Nilges, M., Pannu, N. S., Read, R. J., Rice, L. M., Simonson, T., and Warren, G. L. (1998) Crystallography & NMR system: A new software suite for macromolecular structure determination. *Acta Crystallogr. D54*, 905−921.
(34) Brunger, A. T. (2007) Version 1.2 of the Crystallography and NMR system. *Nat. Protoc. 2*, 2728−2733.
(35) Rieping, W., Habeck, M., Bardiaux, B., Bernard, A., Malliavin, T. E., and Nilges, M. (2007) ARIA2: Automated NOE assignment and data integration in NMR structure calculation. *Bioinformatics 23*, 381−382.
(36) Koradi, R., Billeter, M., and Wuthrich, K. (1996) MOLMOL: A program for display and analysis of macromolecular structures. *J. Mol. Graphics 14*, 29−32 , 51−55.
(37) Laskowski, R. A., Rullmannn, J. A., MacArthur, M. W., Kaptein, R., and Thornton, J. M. (1996) AQUA and PROCHECK-NMR: Programs for checking the quality of protein structures solved by NMR. *J. Biomol. NMR 8*, 477−486.
(38) Hutchinson, E. G., and Thornton, J. M. (1996) PROMOTIF: A program to identify and analyze structural motifs in proteins. *Protein Sci. 5*, 212−220.
(39) De Lano, W. L. (2002) *Pymol*, De Lano Scientific, South San Francisco, CA.
(40) Eswar, N., Webb, B., Marti-Renom, M. A., Madhusudhan, M. S., Eramian, D., Shen, M. Y., Pieper, U., and Sali, A. (2006) Comparative protein structure modeling using Modeller. *Current Protocols in Bioinformatics*, Chapter 5, Unit 5, 6, Wiley, New York.
(41) Shahzad, Z., Ranwez, V., Fizames, C., Marques, L., Le Martret, B., Alassimone, J., Gode, C., Lacombe, E., Castillo, T., Saumitou-Laprade, P., Berthomieu, P., and Gosti, F. (2013) Plant Defensin type 1 (PDF1): Protein promiscuity and expression variation within the *Arabidopsis* genus shed light on zinc tolerance acquisition in *Arabidopsis halleri*. *New Phytol. 200*, 820−833.
(42) Cremer, G. A., Tariq, H., and Delmas, A. F. (2006) Combining a polar resin and a pseudo-proline to optimize the solid-phase synthesis of a 'difficult sequence'. *J. Pept. Sci. 12*, 437−442.
(43) Garcia-Martin, F., White, P., Steinauer, R., Cote, S., Tulla-Puche, J., and Albericio, F. (2006) The synergy of ChemMatrix resin and pseudoproline building blocks renders RANTES, a complex aggregated chemokine. *Biopolymers 84*, 566−575.
(44) Fujiwara, Y., Akaji, K., and Kiso, Y. (1994) Racemization-free synthesis of C-terminal cysteine-peptide using 2-chlorotrityl resin. *Chem. Pharm. Bull. 42*, 724−726.

(45) Barany, G., Han, Y., Hargittai, B., Liu, R. Q., and Varkey, J. T. (2003) Side-chain anchoring strategy for solid-phase synthesis of peptide acids with C-terminal cysteine. *Biopolymers 71*, 652−666.
(46) Hibino, H., and Nishiuchi, Y. (2012) 4-Methoxybenzyloxymethyl group, a racemization-resistant protecting group for cysteine in Fmoc solid phase peptide synthesis. *Org. Lett. 14*, 1926−1929.
(47) Van der Weerden, N. L., and Anderson, M. A. (2013) Plant defensins: Common fold, multiple functions. *Fungal Biology Reviews 26*, 121−131.
(48) De Coninck, B., Cammue, B., and Thevissen, K. (2013) Modes of antifungal action in *planta* functions of plant defensins and defensin-like peptides. *Fungal Biology Reviews 26*, 109−120.
(49) Thevissen, K., Warnecke, D. C., Francois, I. E., Leipelt, M., Heinz, E., Ott, C., Zahringer, U., Thomma, B. P., Ferket, K. K., and Cammue, B. P. (2004) Defensins from insects and plants interact with fungal glucosylceramides. *J. Biol. Chem. 279*, 3900−3905.
(50) Yount, N. Y., and Yeaman, M. R. (2006) Structural congruence among membrane-active host defense polypeptides of diverse phylogeny. *Biochim. Biophys. Acta 1758*, 1373−1386.
(51) Sagaram, U. S., Pandurangi, R., Kaur, J., Smith, T. J., and Shah, D. M. (2011) Structure-activity determinants in antifungal plant defensins MsDef1 and MtDef4 with different modes of action against *Fusarium graminearum*. *PLoS One 6*, e18550.
(52) Thevissen, K., Francois, I. E., Takemoto, J. Y., Ferket, K. K., Meert, E. M., and Cammue, B. P. (2003) DmAMP1, an antifungal plant defensin from dahlia (*Dahlia merckii*), interacts with sphingolipids from *Saccharomyces cerevisiae*. *FEMS Microbiol. Lett. 226*, 169−173.
(53) Poon, I., Baxter, A. A., Lay, F. T., Mills, G. D., Adda, C. G., Payne, J. A., Phan, T. K., Ryan, G. F., White, J. A., Veneer, P. K., van der Weerden, N. L., Anderson, M. A., Kvansakul, M., and Hulett, M. D. (2014) Phosphoinositide-mediated oligomerization of a defensin induces cell lysis. *eLife 3*, e01808.
(54) Thevissen, K., de Mello Tavares, P., Xu, D., Blankenship, J., Vandenbosch, D., Idkowiak-Baldys, J., Govaert, G., Bink, A., Rozental, S., de Groot, P. W., Davis, T. R., Kumamoto, C. A., Vargas, G., Nimrichter, L., Coenye, T., Mitchell, A., Roemer, T., Hannun, Y. A., and Cammue, B. P. (2012) The plant defensin RsAFP2 induces cell wall stress, septin mislocalization and accumulation of ceramides in *Candida albicans*. *Mol. Microbiol. 84*, 166−180.
(55) De Samblanx, G. W., Goderis, I. J., Thevissen, K., Raemaekers, R., Fant, F., Borremans, F., Acland, D. P., Osborn, R. W., Patel, S., and Broekaert, W. F. (1997) Mutational analysis of a plant defensin from radish (*Raphanus sativus* L.) reveals two adjacent sites important for antifungal activity. *J. Biol. Chem. 272*, 1171−1179.
(56) de Medeiros, L. N., Angeli, R., Sarzedas, C. G., Barreto-Bergter, E., Valente, A. P., Kurtenbach, E., and Almeida, F. C. (2010) Backbone dynamics of the antifungal Psd1 pea defensin and its correlation with membrane interaction by NMR spectroscopy. *Biochim. Biophys. Acta 1798*, 105−113.
(57) Craveur, P., Joseph, A. P., Poulain, P., de Brevern, A. G., and Rebehmed, J. (2013) Cis-trans isomerization of omega dihedrals in proteins. *Amino Acids 45*, 279−289.
(58) Meng, H. Y., Thomas, K. M., Lee, A. E., and Zondlo, N. J. (2006) Effects of i and i+3 residue identity on cis-trans isomerism of the aromatic(i+1)-prolyl(i+2) amide bond: Implications for type VI β-turn formation. *Biopolymers 84*, 192−204.
(59) Craik, D. J., Daly, N. L., Bond, T., and Waine, C. (1999) Plant cyclotides: A unique family of cyclic and knotted proteins that defines the cyclic cystine knot structural motif. *J. Mol. Biol. 294*, 1327−1336.
(60) Craik, D. J. (2012) Host-defense activities of cyclotides. *Toxins 4*, 139−156.
(61) Wang, C. K., Wacklin, H. P., and Craik, D. J. (2012) Cyclotides insert into lipid bilayers to form membrane pores and destabilize the membrane through hydrophobic and phosphoethanolamine-specific interactions. *J. Biol. Chem. 287*, 43884−43898.
(62) Tokuriki, N., and Tawfik, D. S. (2009) Protein dynamism and evolvability. *Science 324*, 203−207.
(63) Wouters, M. A., Fan, S. W., and Haworth, N. L. (2010) Disulfides as redox switches: From molecular mechanisms to functional significance. *Antioxid. Redox Signaling 12*, 53−91.
(64) Maret, W. (2006) Zinc coordination environments in proteins as redox sensors and signal transducers. *Antioxid. Redox Signaling 8*, 1419−1441.